RESEARCH ARTICLE | MAY 02 2024

Quantifying the large contribution from orbital Rashba–Edelstein effect to the effective damping-like torque on magnetization

S. Krishnia ; B. Bony; E. Rongione ; L. Moreno Vicente-Arche ; T. Denneulin ; A. Pezo; Y. Lu ; R. E. Dunin-Borkowski ; S. Collin; A. Fert ; J.-M. George ; N. Reyren ; V. Cros ; H. Jaffrès

APL Mater. 12, 051105 (2024)
https://doi.org/10.1063/5.0198970

Quantifying the large contribution from orbital Rashba–Edelstein effect to the effective damping-like torque on magnetization

Cite as: APL Mater. 12, 051105 (2024); doi: 10.1063/5.0198970
Submitted: 20 January 2024 • Accepted: 1 April 2024 •
Published Online: 2 May 2024

S. Krishnia,[1,a] B. Bony,[1] E. Rongione,[1] L. Moreno Vicente-Arche,[1] T. Denneulin,[2] A. Pezo,[1] Y. Lu,[2] R. E. Dunin-Borkowski,[2] S. Collin,[1] A. Fert,[1] J.-M. George,[1] N. Reyren,[1] V. Cros,[1,b] and H. Jaffrès[1,c]

AFFILIATIONS

[1] Laboratoire Albert Fert, CNRS, Thales, Université Paris-Saclay, 91767 Palaiseau, France
[2] Ernst Ruska-Centre for Microscopy and Spectroscopy with Electrons (ER-C 1) and Peter Grünberg Institut (PGI-5), Forschungszentrum Jülich GmbH, 52425 Jülich, Germany

[a] **Current address:** Institute of Physics, Johannes Gutenberg University Mainz, 55099 Mainz, Germany.
[b] **Author to whom correspondence should be addressed:** vincent.cros@cnrs-thales.fr
[c] henri.jaffres@cnrs-thales.fr

ABSTRACT

The generation of large spin currents, and the associated spin torques, which are at the heart of modern spintronics, has long been achieved by charge-to-spin conversion mechanisms, i.e., the spin Hall effect and/or the Rashba–Edelstein effect, intrinsically linked to strong spin–orbit coupling. Recently, a novel path has been predicted and observed for achieving significant current-induced torques originating from light elements, hence possessing weak spin–orbit interaction. These findings point out to the potential involvement of the orbital counterpart of electrons, namely the orbital Hall and orbital Rashba–Edelstein effects. In this study, we aim at quantifying these orbital-related contributions to the effective torques acting on a thin Co layer in different systems. First, we demonstrate in Pt|Co|Cu|AlOx stacking a comparable torque strength coming from the conversion due to the orbital Rashba–Edelstein effect at the Cu|AlOx interface and the one from the effective spin Hall effect in the bottom Pt|Co system. Second, in order to amplify the orbital-to-spin conversion, we investigate the impact of an intermediate Pt layer in Co|Pt|Cu|CuOx. From the Pt thickness dependence of the effective torques determined by harmonic Hall measurements complemented by spin Hall magneto-resistance and THz spectroscopy experiments, we demonstrate that a large orbital Rashba–Edelstein effect is present at the Cu|CuOx interface, leading to a twofold enhancement of the net torques on Co for the optimal Pt thickness. Our findings not only demonstrate the crucial role that orbital currents can play in low-dimensional systems with weak spin–orbit coupling but also reveal that they enable more energy efficient manipulation of magnetization in spintronic devices.

I. INTRODUCTION

The manipulation of magnetization through electrical means at room temperature, usually achieved through torques originating from pure spin current[1–4] and/or non-equilibrium spin density, and involving heavy metals or oxides,[5,6] holds huge potential for energy-efficient and high-speed spintronic device applications. These encompass spin–orbit torque based magnetic random access memory (SOT-MRAM),[7,8] logic gates,[9] skyrmion-based racetracks,[10,11] as well as emerging neuromorphic computing applications.[12–15] However, despite more than one decade of research for current-induced torque optimization, recent observations in systems composed of light elements, i.e., weak spin–orbit interaction, have challenged the conventional understanding regarding their origin.[16–19] In fact, the spin current responsible for these torques was previously uniquely associated with the spin Hall effect (SHE) in heavy 5*d* transition metals (TMs)[20,21] or with the spin Rashba–Edelstein effect at interfaces with broken inversion symmetry,[22] the two effects for which the relativistic spin–orbit coupling (SOC) plays a crucial role. These new findings in systems with weak

SOC represent a paradigm shift by underscoring the significance of both electronic spin and orbital degrees of freedom at equal footing and even accentuate the generation of orbital currents as a potential avenue for a more efficient magnetization manipulation.[23,24]

Notably, the response of orbital angular momentum (OAM) to the application of a charge current has been calculated in certain cases to exceed that of pure spin angular momentum.[25] Very interestingly, unlike spin angular momentum, OAM does not necessarily require SOC, thus expanding the range of materials and interface design possibilities for current-induced magnetization control.[26] In particular, the direct experimental observations of the OAM accumulation in a light element such as titanium,[27] and more recently in chromium,[28] via the orbital Hall effect (OHE), or by the Hanle magnetoresistance effect in manganese,[29] highlight its relevance. Furthermore, clear experimental demonstrations of current-induced torques at inversion-asymmetric light metal/ferromagnet interfaces have provided crucial insights into the non-equilibrium OAM phenomenon.[16,19] Two predominant mechanisms, namely OHE[23] and the orbital Rashba–Edelstein effect (OREE),[16] have been proposed to explain these intriguing observations. On the one hand, OHE entails the flow of helical OAM in opposing directions, perpendicular to the charge current, thereby generating an orbital current. On the other hand, OREE accounts for the accumulation of helical OAM at inversion-asymmetric interfaces. Such orbital current and/or accumulated OAM may subsequently diffuse and propagate within an adjacent layer, being a ferromagnet or a heavy material. This feature has recently been evidenced by the longer orbital current decoherence length[29–32] compared to the corresponding spin length. However, a fundamental difference is that, contrary to spin current, the orbital current itself cannot interact directly with the magnetization through an exchange mechanism and has to involve spin–orbit interactions. In this regard, given the relatively weak SOC of ferromagnetic layers, an intermediate *orbital-to-spin conversion* layer has to be strategically incorporated between the ferromagnetic layer and the orbital current source, e.g., Pt[31,33] or rare-earth elements with strong SOC, such as Gd or Tb.[30,33] Therefore, the overall effectiveness of the torques acting on the magnetic layer hinges on the strength of the spin–orbit interaction (*i*) in the orbital layer or interface, such as air oxidized Cu in Refs. 34 and 35, (*ii*) in the heavy metal spacer layer, and (*iii*) in the ferromagnetic layer. Consequently, a systematic study on new materials is required and it becomes an important issue to be tackled from both fundamental and technological points of view.

In this study, we report on the experimental observation of the strong enhancement of the damping-like (DL) current-induced torques obtained in two types of sputtered multilayers, i.e., Pt|Co|Cu|AlOx and Co|Pt|CuOx samples with respective out-of-plane and in-plane magnetic anisotropy and compared to reference SHE Co|Pt systems. This enhancement of DL torque is explained by the strong OREE at the interface between a light element and an oxide layer. In that sense, this study differs from our recently published work,[19] which focused on the huge exaltation of the field-like torque (FLT) component observed in Pt|Co|Al|Pt systems due to OREE occurring at the ferromagnet–light metal (Co|Al) interface. Furthermore, in the Co|Pt|Cu|CuOx series, we investigate the Pt thickness dependence of the subsequent orbital-to-spin conversion and demonstrate an additional impact on the DL torques. By harnessing such OREE in light transition metal (light-TM) based structures, we achieve a noteworthy twofold enhancement for the effective torques on the Co layer, as validated through harmonic Hall as well as orbital Hall magnetoresistance (OMR) measurements. Our conclusion reveals new aspects of how the orbital properties of conduction electrons may influence the magnetization dynamics, opening up new avenues to control it in future energy-efficient spintronic devices.

II. MATERIAL SYSTEMS EVIDENCING LARGE ORBITAL RASHBA–EDELSTEIN EFFECT

The different multilayers studied in this work have been grown at room temperature using dc magnetron sputtering onto thermally oxidized Si|SiO_2 (280 nm) substrates. A more detailed description of the growth conditions by sputtering deposition and device fabrication can be found elsewhere.[19] The sample series having an Al or a Cu film as a top layer are naturally oxidized in air, thus forming, respectively, AlOx or Al|AlOx and CuOx or Cu|CuOx interfaces depending on the initial thickness of Al or Cu. In the following, these samples will be marked with a star symbol ($*$). Note that for the samples having Pt (3 nm) as a top layer, we know from a previous study using x-ray photo-electron spectroscopy (XPS) characterization that the underlying material, i.e., Al or Cu, is fully protected from oxidization.[19] For electrical and torque measurements, 5 μm wide Hall bar structures are prepared from the multilayers using optical lithography and Ar^+ ion-milling technique.

A. Ta|Pt|Co|Cu|Al* samples with perpendicular magnetic anisotropy

We first investigate the current-induced torques in Ta(5)|Pt(8)|Co(1.4)|Cu(5)|Al*(2) deposited on Si|SiO_2. The number in parentheses indicates the thickness in nm. The results are then compared with the ones obtained in Ta|Pt|Co|Cu|Pt, Ta|Pt|Co|Al|Pt, and Ta|Pt|Co|Al* samples that serve as references for current-induced torque measurements (see also our recent work by Krishnia *et al.*).[19]

1. Experimental determination of the damping-like torque

In order to quantify those current-induced torques, the harmonic Hall measurement technique has been used. In practice, an alternating current (ac) of frequency ω = 727 Hz is injected in the Hall bar that generates orbital and/or spin current and subsequently exerts torques on the magnetization with two contributions: the respective damping-like (DL) and field-like (FL) components. The resultant effective fields induce small quasi-static oscillations of magnetization around their equilibrium position, synchronized with the ac frequency. This dynamic behavior gives rise to a voltage (or resistance) signal at twice the frequency of ac current (2ω). In the case of samples with perpendicular magnetic anisotropy (PMA), we simultaneously make the acquisition of first and second harmonics of the Hall resistance while sweeping the in-plane magnetic field along the current direction (damping-like geometry) or transverse to the current direction (field-like geometry). Note that in the present study, we focus on the analysis of the damping-like effective field (H_{DL}), as we find that it is largely the dominant one for the Pt|Co|Cu|Al* sample under investigation. The in-plane magnetic field dependence of the second harmonic Hall resistance

($R_{2\omega}$) allows us to extract the DL component of the torque and is given by[36]

$$R_{2\omega} = -\frac{1}{2}\sin(\theta)\left(\frac{H_{DL}R_{AHE}}{H_K\cos(2\theta) - H_x\sin(\delta\theta_H - \theta)} + \frac{2H_{FL}R_{PHE}\sec(\delta\theta_H)\sin(\theta)}{H_x}\right), \quad (1)$$

where H_{DL} and H_{FL} are the respective DL and FL effective fields, respectively, H_k is the anisotropy field, H_x is the in-plane magnetic field, θ is the angle of magnetization from the out-of-plane axis, $\delta\theta_H$ is the tilt angle of the in-plane magnetic field, and R_{AHE} and R_{PHE} are the anomalous and planar Hall resistances, respectively. R_{AHE}, θ, H_k, and $\delta\theta_H$ are extracted by fitting the first harmonic Hall resistance using the Stoner–Wohlfarth model as shown in the inset of Fig. 1(a) and as explained in our previous work.[19,36]

In Fig. 1(a), we show the variation in $R_{2\omega}$ as a function of the in-plane magnetic field in the DL geometry for various currents in the Pt(8)|Co(1.4)|Cu(5)|Al*(2) sample along with the fits using Eq. (1). The extracted H_{DL} vs the current density injected in the 8 nm bottom Pt (J_{Pt}) is shown in Fig. 1(b) (red circles). Such a local current density has been evaluated through the measurement of both longitudinal R_{xx} and transverse R_{xy} resistances within a parallel resistor scheme as described hereafter in more detail. The H_{DL} exhibits a linear increase with J_{Pt} and undergoes a sign change relative to the magnetization direction in agreement with symmetry arguments. The interesting outcome lies in the significant variation in H_{DL} magnitude depending on the specific top light-metal interfaces, which are Pt|Co|Cu|Pt, Pt|Co|Al|Pt, and Pt|Co|Al*. First, we find a twofold decrease in H_{DL} in Pt|Co|Cu|Pt (black circles) compared to the two reference samples, i.e., Pt|Co|Al|Pt (orange circles) and Pt|Co|Al* (blue circles). This reduction can be explained, to a large extent, by an opposite SHE contribution from the top 3 nm Pt given the significant electronic and spin transmission across Cu. In our previous work, such a partial compensation in the SHE between bottom and top Pt has been very precisely evaluated to be 60% for a characteristic spin-diffusion length λ_{sf}^{Pt} in Pt of 1.5 nm[19] and 50% for λ_{sf}^{Pt} in Pt of 1.75 nm, as observed here. This result also highlights that a metallic Cu layer, free of any oxide interface, cannot directly contribute significantly to any OHE but rather serves as a current shunting pathway.[19]

A second remarkable result observed in Fig. 1(b) is the twofold increase in H_{DL} in Pt|Co|Cu|Al* (red circles) compared to the reference samples, i.e., Pt|Co|Al|Pt (orange circles) and Pt|Co|Al* (blue circles), which cannot be explained by only considering a contribution from SHE. In this case, it is worth mentioning that the bottom Pt|Co interface remains identical in all these samples, and thus, no significant change in the SHE action originating from the bottom Pt layer is expected. Furthermore, we note that Cu and Al are light metals with negligible spin–orbit interaction, so they are not expected to generate a sizable pure spin current through SHE. However, as discussed previously, recent experimental findings indicate the potential generation of an orbital current at a naturally oxidized Cu|CuOx interface,[31] largely contributing to the overall net torques. Moreover, we have recently reported on SOT properties of Pt(t_1)|Co|Pt(t_2), Pt|Co|Al|Pt, and Pt|Co|Cu|Pt series in which we clearly demonstrated that Pt(8)|Co(1.4)|Al(3)|Pt(3) involving thick Co (1.4 nm) and Al (3 nm) layers can be regarded as a "reference" SHE sample in which the H_{DL} predominantly originates from the SHE in the bottom Pt as played by the simpler Pt|Co bilayer.[19] We may then associate, at this stage, the twofold rise in H_{DL} in Pt|Co|Cu|Al* compared to Pt|Co|Al* and/or Pt|Co|Al|Pt with an orbital current generation at the Cu|Al* interface.

2. Longitudinal magnetoresistance: SMR and/or OMR

In addition to harmonic Hall measurements, we further validate the observed increase in H_{DL} in Pt|Co|Cu|Al* through magnetoresistance (MR) measurements. To this aim, we have measured MR in the so-called spin-Hall magnetoresistance (SMR)

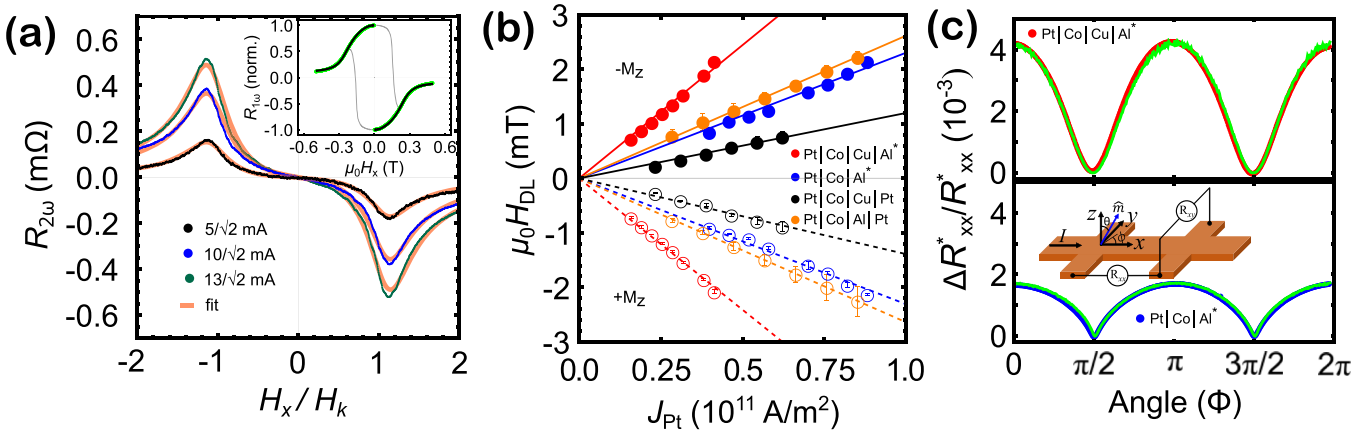

FIG. 1. (a) Second-harmonic Hall resistance ($R_{2\omega}$) as a function of the in-plane magnetic field (H_x), normalized by the anisotropy field (H_k), in Ta(5)|Pt(8)|Co(1.4)|Cu(5)|Al*(2) for three different currents. The solid orange lines represent the fits using Eq. (1). The inset shows the normalized first-harmonic Hall resistance (R_ω) as a function of the in-plane magnetic field and the fit in green using the Stoner–Wohlfarth model. (b) Comparison of H_{DL} as a function of J_{Pt} in Ta(5)|Pt(8)|Co(1.4)|Cu(5)|Al*(2) (red), Ta(5)|Pt(8)|Co(1.4)|Al*(2) (blue), Ta(5)|Pt(8)|Co(1.4)|Al(3)|Pt(3) (orange), and Ta(5)|Pt(8)|Co(1.2)|Cu(1.4)|Pt(3) (black). The H_{DL} values in Ta(5)|Pt(8)|Co(1.2)|Cu(1.4)|Pt(3) are multiplied by a factor of 0.85 to normalize them with 1.4 nm Co thickness. All samples exhibit out-of-plane magnetic anisotropy. The open and filled circles represent two opposite magnetization directions. (c) Spin Hall magneto-resistance measurements, considering the current shunt effects, in Ta(5)|Pt(8)|Co(1.4)|Cu(5)|Al*(2) (top panel) and Ta(5)|Pt(8)|Co(1.4)|Al*(2) (bottom panel) samples. The change in the longitudinal resistance in the same geometry extracted from the anomalous Hall resistance is shown in green (see the text). The schematic of the measurement is also shown.

geometry[37–39] with the current being injected along the $\hat{x}$ direction and $\hat{z}$ is the normal direction to the layers. In this case, the magnetoresistance change, ΔR_{xx} as a function of the angle between the magnetization and the out-of-equilibrium spin or orbital angular momentum polarization direction (generated along the $\hat{y}$ direction), manifests how the angular-momentum current is reflected and/or transmitted at a specific magnetic/non-magnetic interface. Any additional ("*OMR*") contribution originating from the orbital current generated at the Cu|Al* interface shall result in a change in magnetoresistance according to $\frac{\Delta R_{xx}}{R_{xx}} = \frac{\Delta R_{xx}^{SMR}}{R_{xx}^{Pt|Co}} + \frac{\Delta R_{xx}^{OMR}}{R_{OMR}^{Co|top}}$ (here, "*top*" means Al*, Cu|Al*, Cu|Pt, or Al|Pt). We simultaneously measure both the longitudinal (R_{xx}) and transverse (R_{xy}) resistances by rotating the sample in the $(\hat{y}-\hat{z})$ plane under the application of a fixed magnetic field of 670 mT, larger than the anisotropy field [see Fig. 1(c)].

In this geometry, the magnetization consistently remains perpendicular to the direction of the charge current flow, thereby eliminating any contribution from anisotropic magnetoresistance (AMR). Consequently, any variation in ΔR_{xx} solely arises from SMR and/or OMR effects as $\Delta R_{xx} = \Delta R^{SMR+OMR}(1 - m_y^2)$, where $\Delta R^{SMR+OMR}$ is the change of the total MR due to both SMR and OMR according to the relationship $\Delta R^{SMR+OMR} = \Delta R_{xx}(\hat{m}\|\hat{z}\ or\ \hat{m}\perp\hat{\sigma}) - \Delta R_{xx}(\hat{m}\|\hat{y}\ or\ \hat{m}\|\hat{\sigma})$. Here, $\hat{m}$ and $\hat{\sigma}$ are the unit vectors of the magnetization and angular momentum (spin or orbital) polarization directions and m_y is the y component of $\hat{m}$. In Fig. 1(c), we show in red the MR ratio, $\Delta R_{xx}/R_{xx}$ vs the rotation angle for Pt|Co|Cu|Al* (red in the top panel) and for Pt|Co|Al* (blue in the bottom panel). For comparison, we also include in Fig. 1(c) the effective MR from the R_{AHE} data (in green) according to the relationship $\Delta R_{xx}(\theta) = \Delta R^{SMR+OMR}\left(1 - \left(\frac{R_{xy}(\theta)}{R_{AHE}}\right)^2\right)$. The MR variation measured from the two different angular dependences is in excellent agreement, in particular owing to the non-collinearity between magnetization and magnetic field due to the strong anisotropy. The increase in the MR ratio by a factor of more than two between the two samples witnesses the existence of an OAM polarization originating from the Cu|Al* interface. Such orbital accumulation is then after converted either into a charge current in the Co layer or into an intermediate spin-current at the bottom Pt|Co interface by SOC (orbital-to-spin filtering effect in Pt) before being released into a charge current via the inverse spin-Hall effect (ISHE).

B. Co|Pt|Cu* samples with in-plane anisotropy

In this section, we focus on the study of the net DL torques acting on the Co magnetization in Co(2)|Pt(t_{Pt})|Cu*(3) samples exhibiting an in-plane magnetic anisotropy. The Cu*(3) material has been chosen here because of its property to provide helical OAM at its Cu|Ox interface as shown in Refs. 16 and 40 and as displayed from our DFT calculations of the electronic band structure calculations and Rashba–Edelstein response (see Sec. IV of the supplementary material). From the experimental point-of-view, the field required to saturate the magnetization along the out-of-plane direction is about 950 mT (see Sec. III of the supplementary material). Note that for sample series, we deliberately do not include any Ta|Pt buffer layer and directly deposit the multilayers on Si|SiO_2 for avoiding spurious spin-current from any bottom SHE Pt layer, strongly competing with the orbital component. In order to determine the actual impact of orbital currents on the effective torque, we have compared the results with the ones resulting from various non-magnetic metals, including Pt|Cu*, Cu*, Pt, and Pt|Al*. The last two cases are

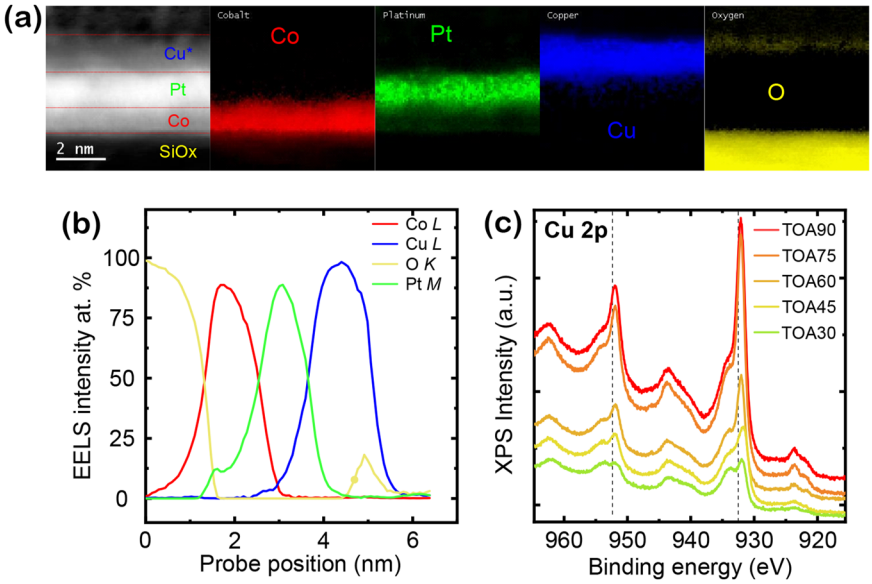

FIG. 2. (a) HAADF STEM image of the Co(2)|Pt(3)|Cu*(3) sample grown in SiOx. The EELS element mapping displaying the spatial elemental distribution of Co (red), Pt (green), Cu (blue), and oxygen (yellow) is also shown. (b) Profiles of atomic fraction of Co (red), Pt (green), Cu (blue), and oxygen (yellow) measured along the growth direction and averaged along the direction parallel to the interfaces. (c) Takeoff angle (TOA) dependence of the XPS spectra in Co(2)|Pt(2)|Cu*(3) for the Cu 2*p* transition. The probing depth increases with TOA being maximum for TOA90.

considered as reference samples. These capping layers serve two primary purposes: first to prevent oxidation of the Co layer and second to act as a source of spin and/or orbital current.

1. Structural and chemical characterization

Concerning this particular series, in which the 2 nm thin Co layer is directly grown on Si|SiO_2, it is essential to get some insights into the structural and chemical properties of the samples in order to corroborate the conclusions revealed from the torque behavior. In Fig. 2(a), we show a cross section image of the Co(2)|Pt(2)|Cu*(3) sample obtained using high-angle annular dark-field scanning transmission electron microscopy (HAADF STEM). The spatial distribution along the thickness for each element, i.e., Co (red), Pt (green), Cu (blue), and oxygen (yellow), obtained using the electron energy loss spectroscopy (EELS) technique is plotted in Fig. 2(b). These EELS data clearly show that, first, each layer is continuous, flat, and homogeneous and, second, only the top part of the Cu layer is oxidized, clearly revealing a pristine Cu of about 1.5 nm thick.

In addition, we have also performed some x-ray photo-electron spectroscopy (XPS) at various takeoff angles (TOAs) in order to gain insights into the distribution of species within the top Cu* layer in Co|Pt|Cu* and Co|Cu* stacks. This TOA corresponds to the angle between the sample surface and the collection axis of the spectrometer: TOA90 is equivalent to normal emission (maximum probing depth) and TOA30 is equivalent to a geometry with a higher degree of inclination (minimum probing depth). In case of a gradient of composition in the Cu* layer, the contribution of near-surface species to the spectrum shall be the largest for the geometry with the shallower probing depth (i.e., TOA30). The evolution of the shape of the XPS spectra at different TOAs shown in Fig. 2(c), notably close to the L_3 edge (around 932 eV), brings some evidence that a spatial variation of the oxidation state is present within the Cu*(3) top layer with a typical distribution being Cu|Cu_2O|Cu$(OH)_2$ along the z-direction. A much more detailed analysis of these XPS characterizations is presented in Sec. I of the supplementary material.

2. Determination of the metallic Cu thickness

Complementary to the EELS and XPS results presented before, the resistance–area product (R_s) and R_{AHE} can also be used to check the presence of a thin metallic Cu layer through the estimation of the shunting current as described within a simple *parallel resistor* scheme. The evolution of the sheet resistance R_s as a function of Pt thickness t_{Pt} is shown is Fig. 3(a) for the two types of samples, i.e., Co(2)|Pt(t_{Pt})|Cu*(3) (2 series) and Co(2)|Pt(t_{Pt}). The slope of $R_s^{-1} = G_s = G_{Pt} + G_{rest} = \sigma_{Pt} t_{Pt} + G_{rest}$ vs t_{Pt} in the inset of Fig. 3(a) gives the Pt resistivity of 27 ± 2 $\mu\Omega$ cm. The shift of the intercept of the linear variation between the two series allows us to extract the product of the Cu*(3) material conductivity times its thickness. From this, we deduce a thickness for the pristine metallic Cu layer to be about 1 nm, considering a typical resistivity ρ_{Cu} = 10 $\mu\Omega$ cm at room temperature. As a corollary to R_s, R_{AHE} may also provide additional information about the current shunt mechanism in a same *parallel resistance* scheme. Indeed, as revealed in Fig. 3(b), the AHE amplitude severely drops as t_{Pt} increases over its typical mean-free path (λ^{Pt}), mainly due to the passive action introduced by the Pt and Cu* layers. From Ref. 41, the standard law of the AHE variation taking into account such current shunting effects reads $R_{AHE}^{Cu*}(\zeta) = \zeta^2 R_{AHE}^{Ref}$, with $\zeta = \frac{R(Cu*)}{R^{(Ref)}}$ being the ratio of the respective resistances with Cu*/and without the additional shunt.[41] This ratio corresponds to the proportion of the CIP-current in the reference AHE system within the whole structure. Such a model aligns well with our experimental results. For instance, in the case for which a 1 nm Cu layer is added to a 2 nm thick Pt current shunt, R_s decreases by a factor of 2, while $R_{AHE} = R_{xy}$ drops by a factor of 4. Similarly, for t_{Pt} = 4 nm, the drop in R_s from ≈78 Ω/□ to ≈50 Ω/□ (ζ = 1.56 and ζ^2 ≈ 2.45) with Cu* inserted leads to a drop of R_{AHE} by ≈2.5 from 1 to 0.4 Ω. The very good overall linearity between R_{AHE} and R_s^{-2} is displayed in the inset of Fig. 3(b). Importantly, it is to be emphasized that this result underlines the good growth quality of the multilayer, i.e., flatness of the layers and limited interdiffusion at interfaces, leading to a well-established spin-dependent two-channel parallel resistor modeling with/without the additional Cu* overlayer.

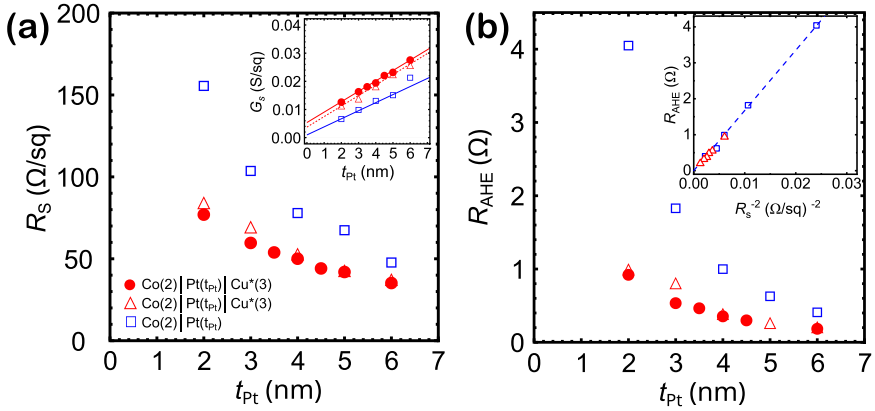

FIG. 3. (a) R_s and (b) R_{AHE} as a function of t_{Pt} in Co(2)|Pt(t_{Pt}) (blue open squares) and in two Co(2)|Pt(t_{Pt})|Cu*(3) series of samples (red solid circles and open triangles). The sheet conductance ($G_s = R_s^{-1}$) is shown in the inset of (a). The inset of (b) shows the relationship between R_{AHE} and R_s for the respective Co(2)|Pt(t_{Pt}) (blue) and Co(2)|Pt(t_{Pt})|Cu*(3) (red) showing the very good linearity of R_{AHE} vs R_s^{-2}.

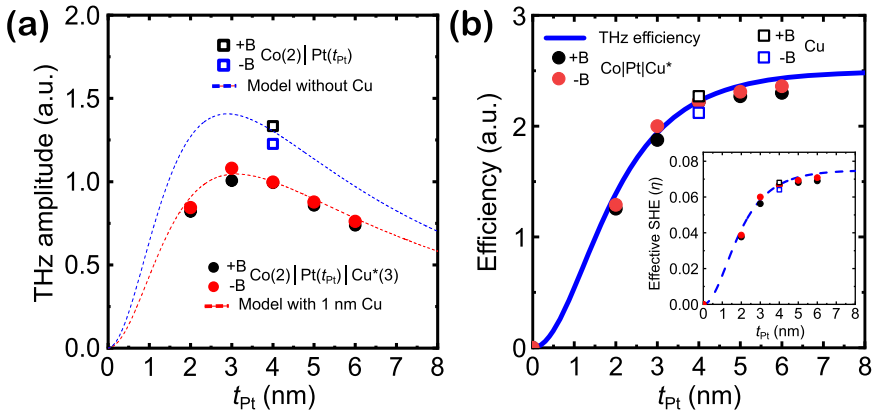

FIG. 4. (a) Amplitude of E_{THz} emitted from Co(2)|Pt(t_{Pt})|Cu*(3) (red and black circles) and Co(2)|Pt(t_{Pt}) (blue and black open squares) as a function of the Pt thickness for an in-plane saturating plane magnetic field $B \simeq 0.1$ T. The respective lines are the fit corresponding to $\eta \times \mathcal{A}$ (see the text). They have been obtained by considering a conductivity of Pt of 4×10^6 S/m (resistivity $\rho_{Pt} = 25\ \mu\Omega$ cm) and a 1 nm conductive Cu layer of conductivity 10^7 S/m (resistivity $\rho_{Cu} = 10\ \mu\Omega$ cm) in Co(2)|Pt(t_{Pt})|Cu*(3). (b) Plot of the η function (inset) exhibiting the efficiency of the spin injection and subsequent THz emission. *Error bars are given by the size of the dots in the plot*.

THz spectroscopy experiments (THz-TDS) in the so-called emission mode are an alternate method to probe the partial metallic character of Cu*. The details of the respective setup and protocol are provided in Sec. II of the supplementary material and in Refs. 41–43. The THz amplitudes obtained vs the Pt thickness are presented in Fig. 4(a), where the black and red points correspond to the absolute value of E_{THz} for the two opposite saturating magnetic fields orientated in the sample plane and corresponding to the +/− THz waveform polarities. The observed shape of the E_{THz} vs t_{Pt} plot results from the product of two functions, respectively, $\eta \times \mathcal{A}$ involving the SCC efficiency η and $\mathcal{A}$ describing the effect of both the THz and near-infrared (NIR) optical absorptions.

The spin–charge conversion efficiency η is a growing function of t_{Pt}, $\eta(t_{Pt}) = \theta_{SHE} \frac{g_{\uparrow\downarrow} r_s \tanh\left(\frac{t_{Pt}}{2\lambda_{sf}^{Pt}}\right)}{1 + g_{\uparrow\downarrow} r_s \coth\left(\frac{t_{Pt}}{\lambda_{sf}^{Pt}}\right)}$ passing through the origin ($\eta = 0$ for $t_{Pt} = 0$), as displayed in Fig. 4(b) (in THz arbitrary unit) and its inset giving the corresponding dependence of the effective spin-Hall angle $\eta = \theta_{SHE}^{eff}$ vs t_{Pt}. λ_{sf}^{Pt} is the hot electron spin relaxation length in Pt, the typical length scale over which the ISHE occurs; $r_s = \rho_{Pt} \times \lambda_{sf}^{Pt}$ is the corresponding spin resistance of Pt[41] (we will further call $\tilde{r}_s = g_{\uparrow\downarrow} r_s$ the reduced spin resistance times the spin-mixing conductance).

Accessing the Pt conductivity responsible for the optical NIR absorption allows us to determine both the thickness and the resistivity of the remaining metallic Cu layer. The estimated values are ~1 nm and 10 $\mu\Omega$ cm. We have checked that the THz signal emitted from a reference sample that does not contain any Cu and/or Cu|Cu* interface [blue and black points in Fig. 4(b) for the two different field polarities] is also well recovered by the same simulation protocol. This ensures the consistency of both measurements and analyses by fixing the hot electron spin relaxation length $\lambda_{sf}^{Pt} = 1.45 \pm 0.05$ nm and $\tilde{r}_s = (g_{\uparrow\downarrow} r_s) = 2$.

3. Quantification of the net DL torques

To quantify the current-induced torques in samples with in-plane magnetic anisotropy, we have measured $R_{1\omega}$ and $R_{2\omega}$ as a function of the angle (ϕ) between the current and magnetization by rotating the sample in the plane, under a constant in-plane magnetic field (H_{ex}). The angular dependence of $R_{2\omega}$ obtained for the Co(2)|Pt(4)|Cu*(3) sample for various currents and a fixed $H_{ex} = 206$ mT is shown in Fig. 5(a). The variation in $R_{2\omega}$ with respect to ϕ arises from a combination of current-induced effective fields, including H_{DL}, H_{FL}, and Oersted (H_{Oe}) effective fields, as well as thermal effects. The angular dependence of $R_{2\omega}$ can be expressed as

$$R_{2\omega} = \left(R_{AHE} \times \frac{H_{DL}}{H_k + H_{ex}} + I\alpha\Delta T\right)\cos(\phi) + 2R_{PHE} \times (2\cos^3(\phi) - \cos(\phi)) \times \frac{H_{FL} + H_{Oe}}{H_{ex}}, \quad (2)$$

where α is the thermal coefficient. In order to separate the two contributions (*resp.* $H_{DL} + I\alpha\Delta T$ and $H_{FL} + H_{Oe}$) appearing in the right-hand side of Eq. (2), we have fitted $R_{2\omega}$ vs ϕ curves with $\cos(\phi)$ by forcing it to cross through the points where the second term vanishes and the $R_{2\omega}$ signal arises solely from H_{DL} plus the thermal effects. The fittings are shown by dotted lines in Fig. 5(a) for several injected currents and corresponding current densities. The residual of the cosine fit simply gives us the $H_{FL} + H_{Oe}$ contribution as shown in the inset of Fig. 5(a) obtained for a current $I = 5/\sqrt{2}$ mA. Since the amplitude of H_{FL} [term in $2\cos(\phi)^3 - \cos(\phi)$ in the right-hand side of Eq. (2)] is one order of magnitude smaller than H_{DL} in all our samples [see the inset of Fig. 5(a)], our primary focus in the subsequent analysis will be on the H_{DL} torque component. In order to disentangle the contribution from thermal effects, we have also measured $R_{2\omega}$ vs. ϕ scans at several external magnetic fields. The slope of the linear fit (dotted lines) yields the

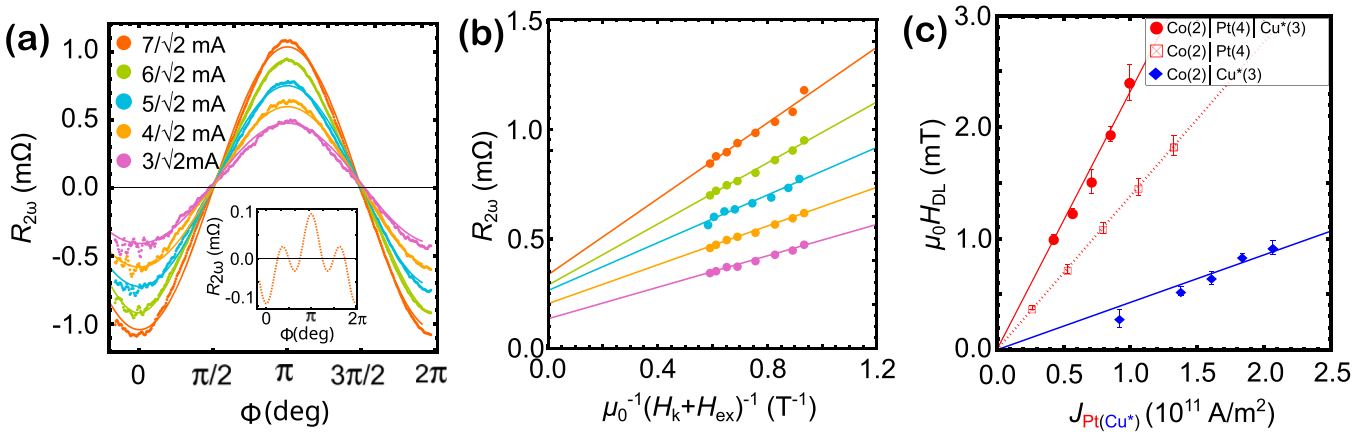

FIG. 5. (a) $R_{2\omega}$ as a function of in-plane angle between injected current and magnetization direction for various currents in the Co(2)|Pt(4)|Cu*(3) sample. The dotted lines are the cosine fits to separate the H_{FL} and H_{Oe} components from the H_{DL} and thermal effects. The residual of cosine fit is shown in the inset. (b) Amplitude of the cosine fit as a function of effective field for different currents. The corresponding linear fits are shown by linearly fitted lines. (c) The H_{DL} as a function of J_{Pt} in Co(2)|Pt(4) (open squares) and Co(2)|Pt(4)|Cu*(3) samples (red solid circles).The H_{DL} values in Co(2)|Cu*(3) sample as a function of current density in Cu* are shown by blue solid circles. *Error bars are estimated by the circle size reported in the plots.*

magnitude of $H_{DL} \times R_{AHE}$, while the intersection corresponds to the thermal contribution ($I\alpha\Delta T$).

In Fig. 5(c), we compare H_{DL} measured in Co|Cu*, Co|Pt|Cu*, and Co|Pt structures as a function of the current density in Pt and in Cu* for samples free of any Pt. First, we find as expected that H_{DL} increases linearly with the current density for all the samples, which confirms the reliability of our measurements. Second, we measure a sizable DL torque on the Co layer in a system without any heavy metal interface, i.e., Co|Cu* sample (blue solid circles). The amplitude of the damping-like effective field is found to be $\mu_0 H_{DL}/J_{Cu}$ ≈0.4 mT/10^{11} A/m^2 current density in the remaining 1 nm metallic Cu. The existence of such a DL torque in Co|Cu* sample hints on the orbital current generation via the orbital Rashba–Edelstein effect at the Cu|CuOx interface that, in turn, propagates into Co before being converted into a spin current via the SOC of Co. This observation agrees with results from previous studies in the NiFe|Cu*,[32,44] CoFeB|Cu*,[40] YIG|Pt|Cu*,[45] or Cu|AlOx bilayer,[16] hence also emphasizing on the absence of any spin–Rashba interactions in these systems. In the same spirit, more recent results demonstrate the orbital transport and orbital conversion at the Cu|oxide (Cu|MgO) interface by OREE following ultrashort optical excitation.[35] A third important result in Fig. 5(c) that has to be emphasized is the observed twofold increase in the H_{DL} amplitude upon capping the Co|Pt (red square) bilayer with Cu* (red circle). We find that the H_{DL} amplitude increases from ≈1.38 mT/(10^{11} A/m^2) in the Co(2)|Pt(4) bilayer structure to ≈2.31 mT/(10^{11} A/m^2) in the Co(2)|Pt(4)|Cu*(3) trilayer for 10^{11} A/m^2 current density in Pt. Thanks to THz-TDS experiments (Fig. 4), we have also checked that such results cannot originate, for example, from a change in the effective conductivity of Pt on adding Cu* on top (compared to Co|Pt| air), which would have for effect to enhance the SHE current.

III. ORBITAL-TO-SPIN CONVERSION IN Pt

A. Amplification of the orbital Rashba–Edelstein effect through insertion of a thin Pt layer

In order to gain deeper insights into the origin of the strong enhancement of H_{DL} in Cu*-based samples, we have performed a systematic investigation of the evolution of $\mu_0 H_{DL}/J_{Pt}$ as a function of t_{Pt} in the Co(2)|Pt(t_{Pt})|Cu*(3) series and compare it to the results in the reference series Co(2)|Pt(t_{Pt}). As shown in Fig. 6(a), the evolution of the normalized DL torque $\mu_0 H_{DL}/J_{Pt}$ for Co(2)|Pt(t_{Pt}) exhibits a steady increase with t_{Pt} that eventually starts to saturate at t_{Pt} = 5 nm (blue open squares). In Fig. 6(a) (black open squares), we also include the evolution of $\mu_0 H_{DL}/J_{Pt}$ with t_{Pt} recorded for the Co(2)|Pt(t_{Pt})|Al*(1) series. Note that this evolution with t_{Pt} followed the same trend as the one obtained from ISHE data obtained from THz-TDS presented in Fig. 4, in which the SHE efficiency vs $\eta(t_{Pt})$ follows the function $\eta(t_{Pt}) = \theta_{SHE} \frac{(g_{\uparrow\downarrow} r_s) \tanh\left(\frac{t_{Pt}}{2\lambda_{sf}^{Pt}}\right)}{1+(g_{\uparrow\downarrow} r_s) \coth\left(\frac{t_{Pt}}{\lambda_{sf}^{Pt}}\right)}$ as previously defined. Note that we have obtained similar evolution in η function vs t_{Pt} in our previous work using a thinner ferromagnetic layer with out-of-plane magnetic anisotropy.[19] From this, we can conclude that the Pt|Al* interface does not play a significant role in contributing to the additional source of DL torques. By fitting the $\mu_0 H_{DL}/J_{Pt}$ vs t_{Pt} plot (dotted line), we are able to determine the spin diffusion length of Pt, $\lambda_{sf}^{Pt} \approx 1.75 \pm 0.05$ nm, slightly larger than the previous value (1.45 nm) as found for optically excited carriers in THz-TDS and the bulk spin Hall angle of Pt, $\theta_{SHE}^{Pt} = 0.21 \pm 0.02$. The obtained parameters (λ_{sf}^{Pt} and θ_{SHE}^{Pt}) from the reference series are found in excellent agreement with our previous studies on a different sample series[19] and with other studies.[46]

While the SOT fields and related parameters in the Co(2)|Pt(t_{Pt}) and Co(2)|Pt(t_{Pt})|Al*(1) series are in very good agreement with previous studies, we observe in Fig. 6(a) a completely distinct behavior when a Cu*(3) layer is deposited on top of Co(2)|Pt(t_{Pt}) bilayers. In order to demonstrate the reproducibility of the observation, we have prepared, and characterized at different time, two series with similar Co(2)|Pt(t_{Pt})|Cu*(3) stacking (deposited on Si|SiO$_2$) that are shown in red circles and triangles in Fig. 6(a). For both of them, we observe a peak in the $\mu_0 H_{DL}/J_{Pt}$ evolution corresponding to a sharp increase with a maximum around t_{Pt} = 4 nm, before dropping down to the same amplitude as of the reference Co|Pt values at t_{Pt} = 5–6 nm. It is

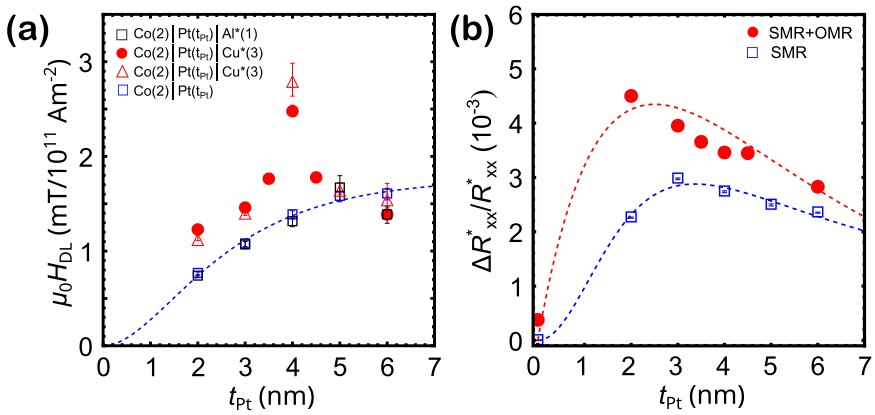

FIG. 6. (a) H_{DL} effective fields normalized by current density in Pt as a function of Pt thickness in Co(2)|Pt(t_{Pt}) (blue open squares), Co(2)|Pt(t_{Pt})|Al*(1) (black open squares), and Co(2)|Pt(t_{Pt})|Cu*(3) (red circles and open triangles). The blue dashed line is the fit corresponding to the function ζ defined in the text. (b) Spin Hall magnetoresistance normalized by the longitudinal resistance and considering the current shunt effects in Co(2)|Pt(t_{Pt})|Cu*(3) (red circles) and Co(2)|Pt(t_{Pt}) (blue open squares), together with the fits in the blue dashed line. The red line is a guide to the eyes calculated from our spin–orbit assisted diffusion model based on Ref. 47.

worth mentioning that we employed a parallel resistance model to calculate the relevant current density injected in the Pt layer estimating its resistivity ≈27 $\mu\Omega$ cm [see Fig. 3(a)]. This sharp enhancement as well the increase in the torque efficiency at smaller Pt thicknesses in Co(2)|Pt(t_{Pt})|Cu*(3) compared to Co(2)|Pt(t_{Pt}) and Co(2)|Pt(t_{Pt})|Al*(1) cannot be understood by considering only spin Hall and/or spin interfacial Rashba–Edelstein effects. In consequence, this brings another unambiguous demonstration that the DL torque enhancement is due to the orbital accumulation generated at the Cu|CuOx interface and subsequently converted into a spin current by an orbital-to-spin conversion through the Pt heavy metal layer.

B. Contribution of the accumulation of orbital angular momentum to the magnetoresistive signal

In order to corroborate the conclusions obtained from the torque measurements, we have also studied the evolution of the longitudinal magnetoresistance (ΔR_{xx}) in the SMR geometry as a function of t_{Pt}. In Fig. 6(b), we present a comparison of the SMR amplitude between Co(2)|Pt(t_{Pt})|Cu*(3) (red solid circles) and Co(2)|Pt(t_{Pt}) (blue open squares) series in order to investigate any additional indirect orbital contribution to the conventional SMR from Co|Pt. In the case of Co|Pt, the evolution of SMR exhibits the expected non-monotonic behavior with respect to t_{Pt}, with an initial increase with t_{Pt}, indicative of the increase in the spin injection efficiency from Pt, and then reaches a peak at t_{Pt} = 3 nm. Subsequently, the SMR decreases for t_{Pt} > 3 nm with a standard $\propto \left(\frac{1}{t_{Pt}}\right)$ law due to current shunting effects for a thicker Pt layer. A typical fitting function $\mathcal{F} = \eta \times \mathcal{I}$ able to reproduce such conventional SMR results is

$$\frac{\Delta R_{xx}^{SMR}}{R_{xx}} = \mathcal{F} = \theta_{SHE}^2 \left(\frac{\lambda_{sf}^{Pt}}{t_{Pt}}\right) \frac{(g_{\uparrow\downarrow} r_s)\ \tanh^2\left(\frac{t_{Pt}}{2\lambda_{sf}}\right)}{1 + (g_{\uparrow\downarrow} r_s)\ \coth\left(\frac{t_{Pt}}{\lambda_{sf}}\right)}, \quad (3)$$

which can then be considered as a product of the spin injection efficiency at the interface η and the so-called *integral function*, $\mathcal{I} = \theta_{SHE}\left(\frac{\lambda_{sf}^{Pt}}{t_{Pt}}\right) \tanh\left(\frac{t_{Pt}}{2\lambda_{sf}}\right)$, describing the total current production in Pt by ISHE from the primary spin-Hall current reflected at the Pt|Co interface. The fitting to the experimental data shown as dashed lines in Fig. 6(b) has been performed by considering λ_{sf}^{Pt} = 1.55 ± 0.05 nm, in pretty close agreement with the THz-TDS and torque data for hot carrier transport. Similar to the Cu|Al* series [see Fig. 1(c)], any additional contribution from the orbital current generated at the Cu|Cu* (or Cu|CuOx) interface may give rise to an enhanced SMR signal according to $\frac{\Delta R_{xx}}{R_{xx}} = \frac{\Delta R_{xx}^{SMR}}{R_{xx}^{Co|Pt}} + \frac{\Delta R_{xx}^{OMR}}{R_{xx}^{Cu*}}$. We observe an increase in $\frac{\Delta R_{xx}}{R_{xx}}$ by about a factor of 2 for t_{Pt} = 2 nm when 3 nm Cu* deposited on top [see Fig. 6(b)]. This MR enhancement, referred to as orbital magnetoresistance (OMR), should be understood as the effect of orbital-to-spin conversion arising in Pt, which aligns well with the torque data. The combined sources of MR, i.e., SMR and OMR, display a typical *bell* curve shape, diminishing at very small Pt thickness as well as at large Pt thickness via the spin dissipation process. Note that the point at t_{Pt} = 0 nm in Fig. 6(b), which yields a non-zero value, corresponds to a pure OMR arising from Co(2)|Cu*(3), and its detailed mechanism should be considered different from the one previously described.

IV. DISCUSSIONS AND CONCLUSIONS

Our thorough investigation of torques and magnetoresistance properties in the Ta|Pt|Co|Cu|Al* and Co|Pt|Cu* series allow us to conclude that both types of oxidized interface with Cu, either Cu|Al* and Pt|Cu*, possess the property to generate sizable OAM, hereafter diffusing into Pt (Co|Pt|Cu*) or into Co (Co|Cu|Al*) to produce enhanced torques. Such OAM generation can be most probably attributed to the interfacial OREE, as shown by density functional theory calculations.[16] Even if bulk Cu itself may also lead to the generation of OAM through OHE, we can exclude such a predominant contribution as the thickness of the metallic Cu remains very small in all our sample series. In our samples, it became clear that the Cu layer

also serves as a transport channel for OAM from its oxidized interface toward the active Co layer within the structure, as emphasized in a previous study.[16]

It is worth noting that one of our striking results is the demonstration of a strong enhancement of spin-orbital torques in Co|Pt|Cu* systems compared to Co|Cu*. This result questions about the inner mechanism of orbital-to-spin conversion occurring in the thin intermediate Pt layer. Even if a precise theoretical description of the experimental results is beyond the scope of the present study, our first modeling points out the particular role played by the *s-d* spin-polarized electronic wave functions in transition metals strongly hybridized as well as related *s-d* diffusion processes, as proposed in the modeling of anisotropic magnetoresistance (AMR) effects.[47]

In conclusion, we have demonstrated the significant role of the orbital Rashba–Edelstein effect to the effective current induced torques in Pt|Co|Cu|Al* and Co|Pt|Cu* (or Co|Pt|Cu|CuOx) structures, revealing previously unexplored facets of the conduction electron behavior. Through a systematic investigation of thickness dependence in the Co|Pt|Cu|CuOx series, we have extracted the key physical parameters, such as the efficiency of spin injection and related spin relaxation lengths as well as additional contributions that we assigned to the orbital component. We have then provided an experimental evidence for the presence of the orbital Rashba–Edelstein effect at the Cu|CuOx interface involving light elements, alongside SHE in Pt. Combining two added contributions allows us to achieve a twofold enhancement in the effective torques acting on the Co magnetization, highlighting the importance of including the electron's orbital degree of freedom in the material strategy to improve drastically the net amplitude of current-induced torques. Beyond the fundamental interest, this insight opens up promising avenues for controlling magnetization in spin-based devices, potentially leading to benefits in terms of energy efficiency and eco-friendly technology applications.

SUPPLEMENTARY MATERIAL

The supplementary material includes a detailed analysis and additional data on the oxidation degree of Cu, an extended analysis of THz-TDS spectroscopy, measurements of anomalous and planar Hall effects, and density functional theory (DFT) simulations of orbital and spin angular momentum transport in Cu|Cu|O and Cu|Al|O structures.

ACKNOWLEDGMENTS

We thank Michel Viret and Jean-Baptiste Moussy (SPEC, Gif-sur-Yvette, France) for fruitful discussions and Sukhdeep Dhillon (LPENS, Paris, France) for his help in THz-TDS spectroscopy measurements. This study has been supported by the French National Research Agency under the Project "ORION" ANR-20-CE30-0022-02, by a France 2030 government grant managed by the French National Research Agency PEPR SPIN ANR-22-EXSP 0007 (SPINMAT), and by the European Horizon Europe Framework Programme for Research and Innovation (2021-2027) EC Grant Agreement No. 101129641 (OBELIX). This work contains results obtained from the experiments performed at the Ernst Ruska-Centre (ER-C) for Microscopy and Spectroscopy with Electrons at the Forschungszentrum Jülich (FZJ) in Germany. The ER-C beamtime access was provided via the DFG Core Facility Project ER-C E-014.

AUTHOR DECLARATIONS

Conflict of Interest

The authors have no conflicts to disclose.

Author Contributions

S. Krishnia: Data curation (equal); Formal analysis (equal); Methodology (equal); Writing – original draft (equal); Writing – review & editing (equal). **B. Bony**: Data curation (equal); Formal analysis (equal); Writing – review & editing (supporting). **E. Rongione**: Investigation (supporting); Writing – review & editing (supporting). **L. Moreno Vicente-Arche**: Formal analysis (supporting); Methodology (supporting); Writing – review & editing (supporting). **T. Denneulin**: Formal analysis (equal); Methodology (supporting); Writing – review & editing (supporting). **A. Pezo**: Formal analysis (equal); Resources (equal); Writing – review & editing (equal). **Y. Lu**: Formal analysis (supporting); Methodology (supporting). **R. E. Dunin-Borkowski**: Resources (supporting); Writing – review & editing (supporting). **S. Collin**: Methodology (supporting); Resources (supporting). **A. Fert**: Formal analysis (supporting); Supervision (supporting); Writing – review & editing (supporting). **J.-M. George**: Data curation (supporting); Writing – review & editing (supporting). **N. Reyren**: Formal analysis (equal); Supervision (supporting); Writing – review & editing (equal). **V. Cros**: Conceptualization (equal); Formal analysis (equal); Funding acquisition (equal); Project administration (equal); Supervision (equal); Validation (equal); Writing – original draft (equal); Writing – review & editing (equal). **H. Jaffrès**: Conceptualization (equal); Data curation (equal); Formal analysis (equal); Funding acquisition (equal); Methodology (equal); Project administration (equal); Supervision (equal); Validation (equal); Writing – original draft (equal); Writing – review & editing (equal).

DATA AVAILABILITY

The data that support the findings of this study are available from the corresponding author upon reasonable request.

REFERENCES

[1] I. M. Miron, K. Garello, G. Gaudin, P.-J. Zermatten, M. V. Costache, S. Auffret, S. Bandiera, B. Rodmacq, A. Schuhl, and P. Gambardella, "Perpendicular switching of a single ferromagnetic layer induced by in-plane current injection," Nature **476**, 189 (2011).

[2] L. Liu, O. J. Lee, T. J. Gudmundsen, D. C. Ralph, and R. A. Buhrman, "Current-induced switching of perpendicularly magnetized magnetic layers using spin torque from the spin hall effect," Phys. Rev. Lett. **109**, 096602 (2012).

[3] L. Liu, C.-F. Pai, Y. Li, H. W. Tseng, D. C. Ralph, and R. A. Buhrman, "Spin-torque switching with the giant spin hall effect of tantalum," Science **336**, 555 (2012).

[4] A. Manchon, J. Železný, I. M. Miron, T. Jungwirth, J. Sinova, A. Thiaville, K. Garello, and P. Gambardella, "Current-induced spin-orbit torques in ferromagnetic and antiferromagnetic systems," Rev. Mod. Phys. **91**, 035004 (2019).

[5] P. Noël, F. Trier, L. M. Vicente Arche, J. Bréhin, D. C. Vaz, V. Garcia, S. Fusil, A. Barthélémy, L. Vila, M. Bibes, and J.-P. Attané, "Non-volatile electric control of spin–charge conversion in a $SrTiO_3$ Rashba system," Nature **580**, 483 (2020).

[6]J. C. R. Sánchez, L. Vila, G. Desfonds, S. Gambarelli, J. P. Attané, J. M. De Teresa, C. Magén, and A. Fert, "Spin-to-charge conversion using Rashba coupling at the interface between non-magnetic materials," Nat. Commun. **4**, 2944 (2013).
[7]V. Kateel, V. Krizakova, S. Rao, K. Cai, M. Gupta, M. G. Monteiro, F. Yasin, B. Sorée, J. De Boeck, S. Couet, P. Gambardella, G. S. Kar, and K. Garello, "Field-free spin–orbit torque driven switching of perpendicular magnetic tunnel junction through bending current," Nano Lett. **23**, 5482 (2023).
[8]N. Figueiredo-Prestes, S. Krishnia, S. Collin, Y. Roussigné, M. Belmeguenai, S. M. Chérif, J. Zarpellon, D. H. Mosca, H. Jaffrès, L. Vila, N. Reyren, and J.-M. George, "Magnetization switching and deterministic nucleation in Co/Ni multilayered disks induced by spin–orbit torques," Appl. Phys. Lett. **119**, 032410 (2021).
[9]K. Raab, M. A. Brems, G. Beneke, T. Dohi, J. Rothörl, F. Kammerbauer, J. H. Mentink, and M. Kläui, "Brownian reservoir computing realized using geometrically confined skyrmion dynamics," Nat. Commun. **13**, 6982 (2022).
[10]A. Fert, V. Cros, and J. Sampaio, "Skyrmions on the track," Nat. Nanotechnol. **8**, 152 (2013).
[11]A. Fert, N. Reyren, and V. Cros, "Magnetic skyrmions: Advances in physics and potential applications," Nat. Rev. Mater. **2**, 17031 (2017).
[12]M. Romera, P. Talatchian, S. Tsunegi, F. Abreu Araujo, V. Cros, P. Bortolotti, J. Trastoy, K. Yakushiji, A. Fukushima, H. Kubota, S. Yuasa, M. Ernoult, D. Vodenicarevic, T. Hirtzlin, N. Locatelli, D. Querlioz, and J. Grollier, "Vowel recognition with four coupled spin-torque nano-oscillators," Nature **563**, 230 (2018).
[13]K. M. Song, J.-S. Jeong, B. Pan, X. Zhang, J. Xia, S. Cha, T.-E. Park, K. Kim, S. Finizio, J. Raabe, J. Chang, Y. Zhou, W. Zhao, W. Kang, H. Ju, and S. Woo, "Skyrmion-based artificial synapses for neuromorphic computing," Nat. Electron. **3**, 148 (2020).
[14]M. Zahedinejad, H. Fulara, R. Khymyn, A. Houshang, M. Dvornik, S. Fukami, S. Kanai, H. Ohno, and J. Åkerman, "Memristive control of mutual spin hall nano-oscillator synchronization for neuromorphic computing," Nat. Mater. **21**, 81 (2022).
[15]P. Sethi, D. Sanz-Hernández, F. Godel, S. Krishnia, F. Ajejas, A. Mizrahi, V. Cros, D. Marković, and J. Grollier, "Compensation of anisotropy in spin hall devices for neuromorphic applications," Phys. Rev. Appl. **19**, 064018 (2023).
[16]J. Kim, D. Go, H. Tsai, D. Jo, K. Kondou, H.-W. Lee, and Y. Otani, "Nontrivial torque generation by orbital angular momentum injection in ferromagnetic-metal/Cu/Al_2O_3 trilayers," Phys. Rev. B **103**, L020407 (2021).
[17]D. Lee, D. Go, H.-J. Park, W. Jeong, H.-W. Ko, D. Yun, D. Jo, S. Lee, G. Go, J. H. Oh, K.-J. Kim, B.-G. Park, B.-C. Min, H. C. Koo, H.-W. Lee, O. Lee, and K.-J. Lee, "Orbital torque in magnetic bilayers," Nat. Commun. **12**, 6710 (2021).
[18]A. El Hamdi, J.-Y. Chauleau, M. Boselli, C. Thibault, C. Gorini, A. Smogunov, C. Barreteau, S. Gariglio, J.-M. Triscone, and M. Viret, "Observation of the orbital inverse Rashba–Edelstein effect," Nat. Phys. **19**, 1855 (2023).
[19]S. Krishnia, Y. Sassi, F. Ajejas, N. Sebe, N. Reyren, S. Collin, T. Denneulin, A. Kovács, R. E. Dunin-Borkowski, A. Fert, J.-M. George, V. Cros, and H. Jaffrès, "Large interfacial Rashba interaction generating strong spin–orbit torques in atomically thin metallic heterostructures," Nano Lett. **23**, 6785 (2023).
[20]I. Mihai Miron, G. Gaudin, S. Auffret, B. Rodmacq, A. Schuhl, S. Pizzini, J. Vogel, and P. Gambardella, "Current-driven spin torque induced by the Rashba effect in a ferromagnetic metal layer," Nat. Mater. **9**, 230 (2010).
[21]A. Manchon, H. C. Koo, J. Nitta, S. M. Frolov, and R. A. Duine, "New perspectives for Rashba spin–orbit coupling," Nat. Mater. **14**, 871 (2015).
[22]Y. A. Bychkov and É. I. Rashba, "Properties of a 2D electron gas with lifted spectral degeneracy," Sov. J. Exp. Theor. Phys. Lett. **39**, 78 (1984).
[23]D. Go, D. Jo, C. Kim, and H.-W. Lee, "Intrinsic spin and orbital hall effects from orbital texture," Phys. Rev. Lett. **121**, 086602 (2018).
[24]D. Go, D. Jo, H.-W. Lee, M. Kläui, and Y. Mokrousov, "Orbitronics: Orbital currents in solids," Europhys. Lett. **135**, 37001 (2021).
[25]L. Salemi and P. M. Oppeneer, "First-principles theory of intrinsic spin and orbital Hall and Nernst effects in metallic monoatomic crystals," Phys. Rev. Mater. **6**, 095001 (2022).
[26]D. Go, J.-P. Hanke, P. M. Buhl, F. Freimuth, G. Bihlmayer, H.-W. Lee, Y. Mokrousov, and S. Blügel, "Toward surface orbitronics: Giant orbital magnetism from the orbital Rashba effect at the surface of sp-metals," Sci. Rep. **7**, 46742 (2017).
[27]Y.-G. Choi, D. Jo, K.-H. Ko, D. Go, K.-H. Kim, H. G. Park, C. Kim, B.-C. Min, G.-M. Choi, and H.-W. Lee, "Observation of the orbital hall effect in a light metal Ti," Nature **619**, 52 (2023).
[28]I. Lyalin, S. Alikhah, M. Berritta, P. M. Oppeneer, and R. K. Kawakami, "Magneto-optical detection of the orbital hall effect in chromium," Phys. Rev. Lett. **131**, 156702 (2023).
[29]G. Sala, H. Wang, W. Legrand, and P. Gambardella, "Orbital Hanle magnetoresistance in a 3*d* transition metal," Phys. Rev. Lett. **131**, 156703 (2023).
[30]G. Sala and P. Gambardella, "Giant orbital Hall effect and orbital-to-spin conversion in 3*d*, 5*d*, and 4*f* metallic heterostructures," Phys. Rev. Res. **4**, 033037 (2022).
[31]S. Ding, A. Ross, D. Go, L. Baldrati, Z. Ren, F. Freimuth, S. Becker, F. Kammerbauer, J. Yang, G. Jakob, Y. Mokrousov, and M. Kläui, "Harnessing orbital-to-spin conversion of interfacial orbital currents for efficient spin-orbit torques," Phys. Rev. Lett. **125**, 177201 (2020).
[32]S. Ding, Z. Liang, D. Go, C. Yun, M. Xue, Z. Liu, S. Becker, W. Yang, H. Du, C. Wang, Y. Yang, G. Jakob, M. Kläui, Y. Mokrousov, and J. Yang, "Observation of the orbital Rashba–Edelstein magnetoresistance," Phys. Rev. Lett. **128**, 067201 (2022).
[33]S. Lee, M.-G. Kang, D. Go, D. Kim, J.-H. Kang, T. Lee, G.-H. Lee, J. Kang, N. J. Lee, Y. Mokrousov, S. Kim, K.-J. Kim, K.-J. Lee, and B.-G. Park, "Efficient conversion of orbital Hall current to spin current for spin-orbit torque switching," Commun. Phys. **4**, 234 (2021).
[34]J. Kim, J. Uzuhashi, M. Horio, T. Senoo, D. Go, D. Jo, T. Sumi, T. Wada, I. Matsuda, T. Ohkubo, S. Mitani, H.-W. Lee, and Y. Otani, "Oxide layer dependent orbital torque efficiency in ferromagnet/cu/oxide heterostructures," Phys. Rev. Mater. **7**, L111401 (2023).
[35]Y. Xu, F. Zhang, A. Fert, H.-Y. Jaffres, Y. Liu, R. Xu, Y. Jiang, H. Cheng, and W. Zhao, "Orbitronics: Light-induced orbital currents in Ni studied by terahertz emission experiments," Nat. Commun. **15**, 2043 (2024).
[36]S. Krishnia, E. Haltz, L. Berges, L. Aballe, M. Foerster, L. Bocher, R. Weil, A. Thiaville, J. Sampaio, and A. Mougin, "Spin-orbit coupling in single-layer ferrimagnets: Direct observation of spin-orbit torques and chiral spin textures," Phys. Rev. Appl. **16**, 024040 (2021).
[37]J. Kim, P. Sheng, S. Takahashi, S. Mitani, and M. Hayashi, "Spin Hall magnetoresistance in metallic bilayers," Phys. Rev. Lett. **116**, 097201 (2016).
[38]Y.-T. Chen, S. Takahashi, H. Nakayama, M. Althammer, S. T. B. Goennenwein, E. Saitoh, and G. E. W. Bauer, "Theory of spin Hall magnetoresistance," Phys. Rev. B **87**, 144411 (2013).
[39]S. Husain, N. Figueiredo-Prestes, O. Fayet, S. Collin, F. Godel, E. Jacquet, N. Reyren, H. Jaffrès, and J.-M. George, "Origin of the anomalous Hall effect at the magnetic insulator/heavy metals interface," Appl. Phys. Lett. **122**, 062403 (2023).
[40]Q. Huang, S. Liu, T. Yang, R. Xie, L. Cai, Q. Cao, W. Lü, L. Bai, Y. Tian, and S. Yan, "Current-induced magnetization switching in light-metal-oxide/ferromagnetic-metal bilayers via orbital Rashba effect," Nano Lett. **23**, 11323 (2023).
[41]T. H. Dang, J. Hawecker, E. Rongione, G. Baez Flores, D. Q. To, J. C. Rojas-Sanchez, H. Nong, J. Mangeney, J. Tignon, F. Godel, S. Collin, P. Seneor, M. Bibes, A. Fert, M. Anane, J.-M. George, L. Vila, M. Cosset-Cheneau, D. Dolfi, R. Lebrun, P. Bortolotti, K. Belashchenko, S. Dhillon, and H. Jaffrès, "Ultrafast spin-currents and charge conversion at 3d–5d interfaces probed by time-domain terahertz spectroscopy," Appl. Phys. Rev. **7**, 041409 (2020).
[42]J. Hawecker, T.-H. Dang, E. Rongione, J. Boust, S. Collin, J.-M. George, H.-J. Drouhin, Y. Laplace, R. Grasset, J. Dong, J. Mangeney, J. Tignon, H. Jaffrès, L. Perfetti, and S. Dhillon, "Spin injection efficiency at metallic interfaces probed by THz emission spectroscopy," Adv. Opt. Mater. **9**, 2100412 (2021).
[43]J. Hawecker, E. Rongione, A. Markou, S. Krishnia, F. Godel, S. Collin, R. Lebrun, J. Tignon, J. Mangeney, T. Boulier, J.-M. George, C. Felser, H. Jaffrès, and S. Dhillon, "Spintronic THz emitters based on transition metals and semi-metals/Pt multilayers," Appl. Phys. Lett. **120**, 122406 (2022).

[44]G. Okano, M. Matsuo, Y. Ohnuma, S. Maekawa, and Y. Nozaki, "Nonreciprocal spin current generation in surface-oxidized copper films," Phys. Rev. Lett. **122**, 217701 (2019).
[45]J. A. Mendoza-Rodarte, M. Cosset-Chéneau, B. J. van Wees, and M. H. D. Guimarães, "Efficient magnon injection and detection via the orbital Rashba Edelstein effect," arXiv:2401.01090 [cond-mat.mes-hall] (2024).
[46]W. Zhang, W. Han, X. Jiang, S.-H. Yang, and S. S P Parkin, "Role of transparency of platinum-ferromagnet interfaces in determining the intrinsic magnitude of the spin Hall effect," Nat. Phys. **11**, 496 (2015).
[47]S. Kokado, M. Tsunoda, K. Harigaya, and A. Sakuma, "Anisotropic magnetoresistance effects in Fe, Co, Ni, Fe_4N, and half-metallic ferromagnet: A systematic analysis," J. Phys. Soc. Jpn. **81**, 024705 (2012).